A New Optimal Reactive Power Flow Model in Rectangular Form and its Solution by Predictor Corrector Primal Dual Interior Point Method

Wei Yan, Juan Yu, David C. Yu, and Kalu Bhattarai

***Abstract*—A new optimal reactive power flow (ORPF) model in rectangular form is proposed in this paper. In this model, the load tap changing (LTC) transformer branch is represented by an ideal transformer and its series impedance with a dummy node located between them. The voltages of the two sides of the ideal transformer are then used to replace the turn ratio of the LTC so that the ORPF model becomes quadratic. The Hessian matrices in this model are constants and need to be calculated only once in the entire optimal process, which speed up the calculation greatly. The solution of the ORPF problem by the predictor corrector primal dual interior point method is described in this paper. Two separate prototypes for the new and the conventional methods are developed in MATLAB in order to compare the performances. The results obtained from the implemented seven test systems ranging from 14 to 1338 buses indicate that the proposed method achieves a superior performance than the conventional rectangular coordinate-based ORPF.**

***Index Terms*—Nonlinear programming, optimal reactive power flow (ORPF), predictor corrector primal dual interior point method (PCPDIPM), sparse techniques.**

I. Introduction

In RECENT years, the predictor corrector primal dual interior point method (PCPDIPM) has been extensively applied to solve large-sized optimal reactive power flow (ORPF) problems [1]–[7], [10]–[12] due to its faster calculation speed and robustness, etc.

The conventional ORPF model in polar coordinates is a higher order problem [5]. Its Hessian matrices are not constants. So the performance of PCPDIPM for solving the ORPF problem will be affected. The alternative approach is a rectangular coordinate-based ORPF model, which represents the ORPF problem in the quadratic functions. The properties of this approach are described in [3] as: 1) its Hessian is a constant; 2) its Taylor expansion terminates at the second-order term without truncation error; and 3) the higher order terms are easily evaluated. Such quadratic features allow for efficient matrix setup and inexpensive incorporation of higher order information in a predictor corrector procedure that reduces the number of IPM iterations for the convergence. Although the voltages in rectangular coordinates are used in [3], the optimal power flow (OPF) formulation is not completely quadratic because of the presence of tap ratio variables in the load tap changing (LTC) branch power equations. A fully quadratic formulation of OPF is proposed in [12]. In that paper, the authors used the current and voltage equations to establish the OPF model in a rectangular form. However, the number of constraints and variables increased so significantly that the advantages of the quadratic model were overwhelmed by the longer time needed for the solution of the higher dimensional system of equations.

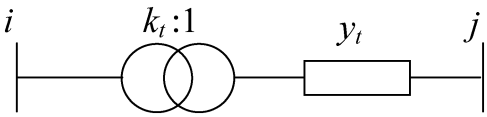

Fig. 1. Ideal transformer circuit of the LTC branch.

In this paper, the LTC branch is represented by an ideal transformer and its series impedance with a dummy node located between them. The voltages of the two sides of the ideal transformer can then replace the tap ratio of LTC to express the branch power. Thus, a new quadratic model for the ORPF problem in a rectangular coordinate is developed. Although the introduction of the dummy nodes will still result in an increase in the number of constraints and variables of the ORPF, this increase is much less in comparison to that in [12]. The test results demonstrate that the emergence of a constant Hessian in the proposed ORPF model greatly reduces the total execution time of the PCPDIPM solution.

This paper is organized as follows. Section II formulates a new ORPF model in the rectangular coordinate system. Section III describes the basic procedure of the PCPDIPM applied to the proposed model. Computational implementation issues are addressed in Section IV. Test results are presented and compared in Section V. Section VI provides the conclusion of this paper.

II. Mathematical Model of ORPF in the Rectangular Coordinates

The transformer branch with LTC can be modeled as an ideal transformer in series with impedance, as shown in Fig. 1, where k_t is the transformer turns ratio, and y_t is the branch admittance.

We can obtain the π equivalent circuit for this LTC branch as shown in Fig. 2.

Manuscript received April 8, 2005; revised August 10, 2005. This work was supported by the Key Laboratory of High Voltage Engineering and the Electrical New Technology, Education Ministry, China. Paper no. TPWRS-00198-2005.

W. Yan and J. Yu are with the Electrical Power Department, Electrical Engineering College, Chongqing University, Chongqing City 400044, China (e-mail: cquyanwei@21cn.com; dianlixi@cqu.edu.cn).

D. C. Yu and K. Bhattarai are with the Electrical Engineering Department, University of Wisconsin-Milwaukee, Milwaukee, WI 53211 USA (e-mail: yu@uwm.edu; kalu@uwm.edu).

Digital Object Identifier 10.1109/TPWRS.2005.861978

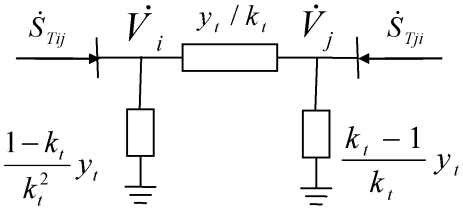

Fig. 2. π equivalent circuit of transformer branch.

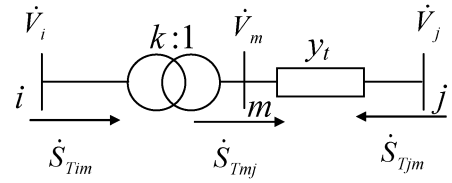

Fig. 3. Ideal transformer circuit with a dummy node.

The branch admittance y_t, branch powers ($\dot{S}_{Tij}$ and $\dot{S}_{Tji}$), and the nodal voltages ($\dot{V}_i$ and $\dot{V}_j$) are expressed in rectangular form as

$$y_t = g_t + jb_t,\ \dot{S}_{Tij} = P_{Tij} + jQ_{Tij},\ \dot{S}_{Tji} = P_{Tji} + jQ_{Tji}$$
$$\dot{V}_i = e_i + jf_i,\ \dot{V}_j = e_j + jf_j.$$

Then, the branch powers and the power losses can be written as

$$P_{Tij} = \frac{g_t}{k_t^2}\left(e_i^2 + f_i^2\right) - \frac{g_t}{k_t}(e_ie_j + f_if_j) + \frac{b_t}{k_t}(e_if_j - e_jf_i) \quad (1)$$

$$Q_{Tij} = \frac{b_t}{k_t}(e_ie_j + f_if_j) - \frac{b_t}{k_t^2}\left(e_i^2 + f_i^2\right) + \frac{g_t}{k_t}(e_if_j - e_jf_i) \quad (2)$$

$$P_{Tji} = g_t\left(e_j^2 + f_j^2\right) - \frac{g_t}{k_t}(e_ie_j + f_if_j) - \frac{b_t}{k_t}(e_if_j - e_jf_i) \quad (3)$$

$$Q_{Tji} = -b_t\left(e_j^2 + f_j^2\right) + \frac{b_t}{k_t}(e_ie_j + f_if_j) - \frac{g_t}{k_t}(e_if_j - e_jf_i) \quad (4)$$

$$\Delta P_{Tij} = \frac{g_t}{k_t^2}\left(e_i^2 + f_i^2\right) + g_t\left(e_j^2 + f_j^2\right) - \frac{2g_t}{k_t}(e_ie_j + f_if_j). \quad (5)$$

From (1)–(5), it can be seen that the branch power equations of the LTC branch in rectangular coordinate system are no longer quadratic because of the tap ratio variable k_t. Even though the rest of the branch power equations are still quadratic, the higher order terms above will diminish the advantages of the rectangular-based ORPF.

In the proposed formulation, a dummy node m is added between the ideal transformer and the series impedance, as shown in Fig. 3. The voltage of the dummy node and the branch power from the dummy node to the impedance are introduced to describe the relationships between the voltages and the branch powers associated with the LTC branch. For the ideal transformer, there are no power losses in between its two terminal nodes i and m; the ratio of the nodal voltage magnitudes is equal to the transformer turns ratio; and the nodal voltage angles of both the nodes are equal. These relationships are described in the following:

$$P_{Tij} = P_{Tmj}, \quad Q_{Tij} = Q_{Tmj} \quad (6)$$

$$k_t = \sqrt{\frac{e_i^2 + f_i^2}{e_m^2 + f_m^2}} \quad (7)$$

$$arctg\left(\frac{f_i}{e_i}\right) = arctg\left(\frac{f_m}{e_m}\right). \quad (8)$$

Now, the branch flow between m and j can be modeled as a regular line flow. As (6) represents a lossless ideal transformer between i and m, the branch power equations of the LTC transformer can then be modified as follows:

$$P_{Tij} = P_{Tmj} = \left(e_m^2 + f_m^2 - e_me_j - f_mf_j\right) g_t + (e_mf_j - e_jf_m)b_t \quad (9)$$

$$Q_{Tij} = Q_{Tmj} = -\left(e_m^2 + f_m^2 - e_me_j - f_mf_j\right) b_t + (e_mf_j - e_jf_m)g_t \quad (10)$$

$$P_{Tji} = P_{Tjm} = \left(e_j^2 + f_j^2 - e_me_j - f_mf_j\right) g_t + (e_jf_m - e_mf_j)b_t \quad (11)$$

$$Q_{Tji} = Q_{Tjm} = -\left(e_j^2 + f_j^2 - e_me_j - f_mf_j\right) b_t + (e_jf_m - e_mf_j)g_t \quad (12)$$

$$\Delta P_{Tij} = \Delta P_{Tmj} = \left(e_m^2 + f_m^2 + e_j^2 + f_j^2 - 2e_me_j - 2f_mf_j\right) g_t. \quad (13)$$

From (9)–(13), it can be seen that the branch power flow equations of the LTC transformer become quadratic similar to the general impedance branches. Equations (9) and (10) show the branch power flow from the high voltage side of the transformer to the low voltage side, whereas (11) and (12) show the branch power flow from the low voltage side of the transformer to the high voltage side. There are no losses in between the high voltage node and the dummy node.

The nodal power equations can be written as in (14) and (15). S_{Li} is the set of all general branches connected to node i, S_{Ti} is the set of all the LTC branches connected to node i, N_B is the number of original system nodes, and P_i and Q_i are the bus active and reactive power injections

$$P_i = \sum_{j \in S_{Li}} P_{Lij} + \sum_{j \in S_{Ti}} P_{Tij} \quad i = 1, \cdots, N_B \quad (14)$$

$$Q_i = \sum_{j \in S_{Li}} Q_{Lij} + \sum_{j \in S_{Ti}} Q_{Tij} \quad i = 1, \cdots, N_B. \quad (15)$$

The new nodal power equations can be derived from (14) and (15) as

$$P_i=\sum_{j=1}^{N_B}[G_{ij}(e_ie_j+f_if_j)+B_{ij}(f_ie_j-e_if_j)]+\sum_{j\in S_{Ti}}P_{Tij} \quad (16)$$

$$Q_i=\sum_{j=1}^{N_B}[G_{ij}(f_ie_j-e_if_j)-B_{ij}(e_ie_j+f_if_j)]+\sum_{j\in S_{Ti}}Q_{Tij} \quad (17)$$

where G_{ij} is the ith row and jth column element of the bus conductance matrix $\boldsymbol{G}$, and B_{ij} is the ith row and jth column element of the bus susceptance matrix $\boldsymbol{B}$, excluding the LTC branches. P_{Tij} and Q_{Tij} are the LTC branch powers connected to node i. When node i is the high voltage side of LTC, P_{Tij} and Q_{Tij} are described by using (9) and (10). When node i is the low voltage side of LTC, P_{Tij} and Q_{Tij} are described by using (11) and (12), where i and j in these equations are switched.

Based on (6)–(17), a new quadratic model of ORPF is proposed as shown in (18)–(26). N_G, N_{cr}, and NT denote the number of the generator nodes, the reactive compensation nodes, and the LTC branches, respectively; Ns is the swing bus; P_i, Q_i (for the node i), and P_{Ns} (for the swing) represent the bus power injections that are defined in (16) and (17); P_{Di}, Q_{Di}, and P_{Gi} are the fixed powers of the load and the generator; Q_{gi} and Q_{cri} represent the controllable reactive power injections by the generator and the compensator; and $(.)_{\max}$ and $(.)_{\min}$ represent the maximum and the minimum limits of (.), respectively

$$\min\ f(\boldsymbol{x})=P_{Ns} \quad (18)$$

s.t.

$$g_{Pi}(\boldsymbol{x})=P_{Gi}-P_{Di}=P_i \quad i=1,\cdots,N_B\ but\quad i\neq Ns \quad (19)$$

$$g_{Qi}(\boldsymbol{x})=Q_{Gi}+Q_{cri}-Q_{Di}=Q_i \quad i=1,\cdots,N_B \quad (20)$$

$$g_{\theta j}(\boldsymbol{x})=e_if_m-e_mf_i=0 \quad j=1,\cdots,N_T \quad (21)$$

$$0\le h_{kj}(\boldsymbol{x})=k_{t\max}^2\left(e_m^2+f_m^2\right)-\left(e_i^2+f_i^2\right) \quad j=1,\cdots,N_T \quad (22)$$

$$0\le h_{kj}(\boldsymbol{x})=\left(e_i^2+f_i^2\right)-k_{t\min}^2\left(e_m^2+f_m^2\right) \quad j=1,\cdots,N_T \quad (23)$$

$$V_{i\min}^2\le h_{Vi}(\boldsymbol{x})=e_i^2+f_i^2\le V_{i\max}^2 \quad i=1,\cdots,N_B \quad (24)$$

$$Q_{Gi\min}\le h_{gi}(\boldsymbol{x})=Q_{Gi}\le Q_{Gi\max} \quad i=1,\cdots,N_G \quad (25)$$

$$Q_{cri\min}\le h_{Ci}(\boldsymbol{x})=Q_{cri}\le Q_{cri\max} \quad i=1,\cdots,N_{cr}. \quad (26)$$

The objective function in (18) is the active power injection P_{Ns} at the swing bus. The bus active and reactive power balance constraints are described in (19) and (20). Equations (21)–(23) deal with the LTC parameters. They replace the transformer turns ratio k_t in the conventional ORPF in rectangular coordinates. This is the key feature of the proposed model. Equation (21) illustrates that the voltage angles are identical between the high voltage node and the dummy node. Equations (22) and (23) are the bound constraints of the transformer turns ratio. The detail derivations of these equations are shown in the Appendix. Equations (24)–(26) represent the bus voltage, the generator, and reactive compensator bound constraints. Due to the introduction of the dummy nodes into the system, all the equations in the proposed ORPF model turn into quadratic. This change will result in constant Hessian matrices in the model and simplify the computation of the Jacobian matrices. However, there are also some drawbacks in the model. By replacing the turn ratio with the voltages of the dummy nodes, the number of constraints and the variables will increase by N_T in the proposed model. The tap ratio limit becomes a quadratic constraint, in contrast to the simple bound limit in the conventional model. Consequently, there is an increase in the number of Lagrange multipliers in the PCPDIPM algorithm, which, in turn, needs more time for solving the larger Newton systems in every iteration. Nevertheless, the results shown in the later sections demonstrate that the time saved in dealing with the constant Hessian matrices is more than the time increased in solving the Newton system.

III. PCPDIPM FOR ORPF

The new model for the reactive power optimization in (18)–(26) can be generalized as the following standard form:

$$\begin{aligned}\min\quad & f(\mathbf{x})\\ \text{s.t.}\quad & \mathbf{g}(\mathbf{x})=\mathbf{0}\\ & \mathbf{h}_1(\mathbf{x})\le\mathbf{h}_{1\max}\\ & \mathbf{h}_2(\mathbf{x})\ge\mathbf{h}_{2\min}\end{aligned} \quad (27)$$

where $f(\mathbf{x})$ represents the objective function; $\boldsymbol{g}(\cdot)$ represents the functions of $\boldsymbol{g}_P$, $\boldsymbol{g}_Q$, and $\boldsymbol{g}_\theta$ in equality constraints functions in (19)–(21); $\boldsymbol{h}_1(\cdot)$ and $\boldsymbol{h}_2(\cdot)$ represent the functions of $\boldsymbol{h}_k$, $\boldsymbol{h}_V$, $\boldsymbol{h}_g$, and $\boldsymbol{h}_C$ in inequality constraints functions in (22)–(26); $\boldsymbol{h}_{1\max}$ and $h_{2\min}$ are the upper and lower bounds in inequality (22)–(26); and $\boldsymbol{x}=[\boldsymbol{e},\boldsymbol{f},\boldsymbol{Q}_g,\boldsymbol{Q}_{cr}]$ is the vector of optimization variables in the ORPF problem.

The ORPF problem in (27) can be solved by a PCPDIPM as mentioned in [3]–[5]. In this method, the slack variables and the Lagrange multipliers are introduced to deal with the inequality and equality constraints, and the logarithmic barrier functions are used to guarantee the nonnegativity conditions of the slack variables. The ORPF problem can be transformed into the subproblem of the Lagrange function L_μ without the constraints

$$\begin{aligned}L_\mu=&f(\boldsymbol{x})-\boldsymbol{y}^T\boldsymbol{g}(\boldsymbol{x})+\boldsymbol{Z}_1^T\left(\boldsymbol{h}_1(\boldsymbol{x})+\boldsymbol{S}_1-\boldsymbol{h}_{1\max}\right)\\ &-\boldsymbol{Z}_2^T\left(\boldsymbol{h}_2(\boldsymbol{x})-\boldsymbol{S}_2-\boldsymbol{h}_{2\min}\right)-\mu\sum_{j=1}^{n1}\ln\boldsymbol{S}_{1j}-\mu\sum_{j=1}^{n2}\ln\boldsymbol{S}_{2j}\end{aligned} \quad (28)$$

where $\boldsymbol{y}\in\boldsymbol{R}^n$, $\boldsymbol{Z}_1\in\boldsymbol{R}^{n1}$, and $\boldsymbol{Z}_2\in\boldsymbol{R}^{n2}$ are the vectors of Lagrange multipliers for the equality and inequality constraints; $\boldsymbol{S}_1\in\boldsymbol{R}^{n1}$ and $\boldsymbol{S}_2\in\boldsymbol{R}^{n2}$ are the vectors of slack variables; n, $n1$, and $n2$ are the number of $g_i(\boldsymbol{x})$, $h_{1i}(\boldsymbol{x})$, and $h_{2i}(\boldsymbol{x})$, respectively; and μ is the barrier parameter.

Based on the Karush–Kuhn–Tucker (KKT) first-order conditions of the subproblem, a set of nonlinear algebraic equations is formed and then solved by the Newton–Raphson algorithm.

In the PCPDIPM, the solution process is divided into two steps: the predictor and the corrector steps in each iteration. In the predictor step, the predicting Newton system is formed according to the first derivatives of KKT equations with μ and the second-order delta terms being equal to zero. The solution of the Newton system is called the affine scaling direction, which is used to predict μ and to estimate the second-order nonlinear terms. In the corrector step, the correcting Newton system is formed with the inclusion of μ and the nonlinear terms calculated from the predicting Newton system. Then, the actual search direction can be obtained by solving this correcting Newton system.

The correcting Newton system can be expressed as follows:

$$\begin{bmatrix} \boldsymbol{H}_H & -\boldsymbol{J}_g^T & \boldsymbol{J}_{h_1}^T & -\boldsymbol{J}_{h_2}^T & 0 & 0 \\ -\boldsymbol{J}_g & 0 & 0 & 0 & 0 & 0 \\ \boldsymbol{J}_{h_1} & 0 & 0 & 0 & \boldsymbol{I}_1 & 0 \\ -\boldsymbol{J}_{h_2} & 0 & 0 & 0 & 0 & \boldsymbol{I}_2 \\ 0 & 0 & \mathrm{diag}\boldsymbol{S}_1 & 0 & \mathrm{diag}\boldsymbol{Z}_1 & 0 \\ 0 & 0 & 0 & \mathrm{diag}\boldsymbol{S}_2 & 0 & \mathrm{diag}\boldsymbol{Z}_2 \end{bmatrix} \times \begin{bmatrix} \Delta\boldsymbol{x} \\ \Delta\boldsymbol{y} \\ \Delta\boldsymbol{Z}_1 \\ \Delta\boldsymbol{Z}_2 \\ \Delta\boldsymbol{S}_1 \\ \Delta\boldsymbol{S}_2 \end{bmatrix} = \begin{bmatrix} -\nabla_x \boldsymbol{L}_\mu \\ \boldsymbol{g}(\boldsymbol{x}) \\ -\boldsymbol{h}_1(\boldsymbol{x}) - \boldsymbol{S}_1 + \boldsymbol{h}_{1\max} \\ \boldsymbol{h}_2(\boldsymbol{x}) - \boldsymbol{S}_2 - \boldsymbol{h}_{2\min}) \\ -\boldsymbol{Z}_1 * \boldsymbol{S}_1 + \boldsymbol{\mu}_1 - \Delta\boldsymbol{Z}_1 * \Delta\boldsymbol{S}_1 \\ -\boldsymbol{Z}_2 * \boldsymbol{S}_2 + \boldsymbol{\mu}_2 - \Delta\boldsymbol{Z}_2 * \Delta\boldsymbol{S}_2 \end{bmatrix} \tag{29}$$

where $\boldsymbol{J}_g \in \boldsymbol{R}^{n\times n}$, $\boldsymbol{J}_{h_1} \in \boldsymbol{R}^{n1\times n1}$, and $\boldsymbol{J}_{h_2} \in \boldsymbol{R}^{n2\times n2}$ are Jacobian matrices of $\boldsymbol{g}(\cdot)$, $\boldsymbol{h}_1(\cdot)$, and $\boldsymbol{h}_2(\cdot)$, respectively; $\boldsymbol{\mu}_1 \in \boldsymbol{R}^{n1}$ and $\boldsymbol{\mu}_2 \in \boldsymbol{R}^{n2}$ are the vectors with their components being μ; diag$\boldsymbol{S}_1$, diag$\boldsymbol{S}_2$, diag$\boldsymbol{Z}_1$, and diag$\boldsymbol{Z}_2$ are diagonal matrices defined by the elements in the vectors $\boldsymbol{S}_1, \boldsymbol{S}_2, \boldsymbol{Z}_1$, and $\boldsymbol{Z}_2$, respectively; "and $*$" represents the *multiplication* of two vectors. The result is also a vector with its element in a particular row being the product of the elements in the same rows of both the vectors

$$\begin{aligned} \nabla_x \boldsymbol{L}_\mu &= \nabla \boldsymbol{f}(\boldsymbol{x}) - \boldsymbol{J}_g(\boldsymbol{x})^T \boldsymbol{y} + \boldsymbol{J}_{h_1}(\boldsymbol{x})^T \boldsymbol{Z}_1 \\ &\quad - \boldsymbol{J}_{h_2}(\boldsymbol{x})^T \boldsymbol{Z}_2 \end{aligned} \tag{30}$$

$$\begin{aligned} \boldsymbol{H}_H &= \boldsymbol{H}_f(\boldsymbol{x}) - \sum_{j=1}^{n} y_j \boldsymbol{H}_{g_j}(\boldsymbol{x}) + \sum_{j=1}^{n1} Z_{1j} \boldsymbol{H}_{h_{1j}}(\boldsymbol{x}) \\ &\quad - \sum_{j=1}^{n2} Z_{2j} \boldsymbol{H}_{h_{2j}}(\boldsymbol{x}) \end{aligned} \tag{31}$$

where $\boldsymbol{H}_f(x), \boldsymbol{H}_{g_j}(x), \boldsymbol{H}_{h_{1j}}(x)$, and $\boldsymbol{H}_{h_{2j}}(x)$ are Hessian matrices of functions $f(\boldsymbol{x})$, $g_j(\boldsymbol{x})$, $h_{1j}(\boldsymbol{x})$, and $h_{2j}(\boldsymbol{x})$, respectively. $\nabla \boldsymbol{f}(x)$ is the gradient of $f(\boldsymbol{x})$.

If the barrier parameter μ and the second-order delta terms $\Delta\mathbf{Z}_1 * \Delta\mathbf{S}_1$ and $\Delta\mathbf{Z}_2 * \Delta\mathbf{S}_2$ are zero, then (29) will represent the predicting Newton system. The delta terms estimated by this equation, called the affine scaling directions, are denoted by the superscript aff.

Equation (29) can be reduced into the following:

$$\begin{bmatrix} \mathbf{H} & -\mathbf{J}_g^T \\ -\mathbf{J}_g & \mathbf{0} \end{bmatrix} \begin{bmatrix} \Delta\mathbf{x} \\ \Delta\mathbf{y} \end{bmatrix} = \begin{bmatrix} \boldsymbol{\psi} \\ \mathbf{g}(\mathbf{x}) \end{bmatrix} \tag{32}$$

where

$$\boldsymbol{H} = \boldsymbol{H}_H + \boldsymbol{H}_J \tag{33}$$

$$\begin{aligned} \boldsymbol{H}_J &= \boldsymbol{J}_{h_1}(\boldsymbol{x})^T \left(\mathrm{diag}\boldsymbol{S}_1^{-1}\mathrm{diag}\boldsymbol{Z}_1\right) \boldsymbol{J}_{h_1}(\boldsymbol{x}) \\ &\quad + \boldsymbol{J}_{h_2}(\boldsymbol{x})^T \left(\mathrm{diag}\boldsymbol{S}_2^{-1}\mathrm{diag}\boldsymbol{Z}_2\right) \boldsymbol{J}_{h_2}(\boldsymbol{x}) \end{aligned} \tag{34}$$

$$\begin{aligned} \boldsymbol{\psi} = &-\nabla_x \boldsymbol{L}_\mu - \boldsymbol{J}_{h_1}(\boldsymbol{x})^T \mathrm{diag}\boldsymbol{S}_1^{-1} \\ &\times \left[-\boldsymbol{Z}_1 * \boldsymbol{S}_1 - \Delta\boldsymbol{Z}_1^{aff} * \Delta\boldsymbol{S}_1^{aff} + \boldsymbol{\mu}_1 \right. \\ &\quad \left. + \mathrm{diag}\boldsymbol{Z}_1 \left(\boldsymbol{h}_1(\boldsymbol{x}) + \boldsymbol{S}_1 - \boldsymbol{h}_{1\max}\right)\right] \\ &+ \boldsymbol{J}_{h_2}(\boldsymbol{x})^T \mathrm{diag}\boldsymbol{S}_2^{-1} \\ &\times \left[-\boldsymbol{Z}_2 * \boldsymbol{S}_2 + \boldsymbol{\mu}_2 - \Delta\boldsymbol{Z}_2^{aff} * \Delta\boldsymbol{S}_2^{aff} \right. \\ &\quad \left. - \mathrm{diag}\boldsymbol{Z}_2 \left(\boldsymbol{h}_2(\boldsymbol{x}) - \boldsymbol{S}_2 - \boldsymbol{h}_{2\min}\right)\right]. \end{aligned} \tag{35}$$

From $\Delta\boldsymbol{x}$, $\Delta\boldsymbol{y}$ terms given by (32), compute

$$\begin{cases} \Delta\mathbf{S}_1 = -\mathbf{J}_{h_1}(\mathbf{x})\Delta\mathbf{x} - \mathbf{h}_1(\mathbf{x}) - \mathbf{S}_1 + \mathbf{h}_{1\max} \\ \Delta\mathbf{S}_2 = \mathbf{J}_{h_2}(\mathbf{x})\Delta\mathbf{x} + \mathbf{h}_2(\mathbf{x}) - \mathbf{S}_2 - \mathbf{h}_{2\min}) \\ \Delta\mathbf{Z}_1 = \mathrm{diag}\mathbf{S}_1^{-1}\left(-\mathbf{Z}_1 * \mathbf{S}_1 + \boldsymbol{\mu}_1 - \Delta\mathbf{Z}_1^{aff} \right. \\ \qquad \left. * \Delta\mathbf{S}_1^{aff} - \mathrm{diag}\mathbf{Z}_1\Delta\mathbf{S}_1\right) \\ \Delta\mathbf{Z}_2 = \mathrm{diag}\mathbf{S}_2^{-1}\left(-\mathbf{Z}_2 * \mathbf{S}_2 + \boldsymbol{\mu}_2 - \Delta\mathbf{Z}_2^{aff} \right. \\ \qquad \left. * \Delta\mathbf{S}_2^{aff} - \mathrm{diag}\mathbf{Z}_2\Delta\mathbf{S}_2\right). \end{cases} \tag{36}$$

IV. Computational Implementation

A. Calculation Procedure for the Constant Hessians

The unique feature of this model is the constant Hessian matrices for all the functions: the objective function, the equality constraints, and the inequality constraints, also including the elements corresponding to the LTC branches. From (31), it can be seen that $\boldsymbol{H}_H$ is the linear combination of the Hessians and the multipliers. The multipliers being variables make $\boldsymbol{H}_H$ not a constant matrix, and it needs to be updated in every iteration. However, the constant Hessians will save a significant amount time in forming the $\boldsymbol{H}_H$.

The way of determining $\boldsymbol{H}_H$ in the proposed method is similar to the conventional method in [3], except that the latter method requires updating the Hessian elements corresponding to the LTC branches in each iteration of the optimization calculation. Therefore, the conventional method needs more time for formulating $\boldsymbol{H}_H$. A detail description of how to construct the $\boldsymbol{H}_H$ matrix is described below.

According to the proposed model, each bus has three Hessians in the composition of $\boldsymbol{H}_H$. One Hessian is associated with constraints (18) or (19), the second with constraint (20), and the other with constraint (24).

- For each $i \in \{1, 2, \ldots, N_B\}$ and all $j \in N_i \geq i$ (N_i is the nonzero column indices in the ith row of bus admittance matrix ($\boldsymbol{G}$ or $\boldsymbol{B}$) without the consideration of the LTC)

$$H_{Hee}(i,i) = H_{Hff}(i,i) = 2\left(G_{ii}\lambda_i^p - B_{ii}\lambda_i^q + \lambda_i^v\right) \quad (37)$$

$$H_{Hee}(i,j) = H_{Hff}(i,j) = G_{ij}\left(\lambda_i^p + \lambda_j^p\right) - B_{ij}\left(\lambda_i^q + \lambda_j^q\right) \quad (38)$$

$$H_{Hfe}(i,j) = B_{ij}\left(\lambda_i^p - \lambda_j^p\right) + G_{ij}\left(\lambda_i^q - \lambda_j^q\right) \quad (39)$$

$$H_{Hef}(i,j) = -B_{ij}\left(\lambda_i^p - \lambda_j^p\right) - G_{ij}\left(\lambda_i^q - \lambda_j^q\right). \quad (40)$$

- The two terminal nodes of the LTC branch may have connections to other general line branches, so the elements of $\boldsymbol{H}_H$ corresponding to these terminal nodes should include two parts. The first part, representing the general branches, is computed from the bus power balance constraints, as in (37). The second part, representing the LTC branches, is the second-order partial derivative of the branch power constraints of the LTC given in (9)–(12). These two parts need to be added together, as shown in (41) and (42). So for each transformer branch shown in Fig. 3 with the node i, dummy node m and j with branch admittance g_{Tij} and b_{Tij}, the corresponding elements in $\boldsymbol{H}_H$ can be computed as follows:

$$\begin{aligned} H_{Hee}(i,i) &= H_{Hff}(i,i) \\ &= H_{Hee}(i,i) + 2\left(\lambda_{t2}^k - \lambda_{t1}^k\right) \end{aligned} \quad (41)$$

$$\begin{aligned} H_{Hee}(j,j) &= H_{Hff}(j,j) \\ &= H_{Hee}(j,j) + 2\left(g_{Tij}\lambda_j^p - b_{Tij}\lambda_j^q\right) \end{aligned} \quad (42)$$

$$\begin{aligned} H_{Hee}(m,m) &= H_{Hff}(m,m) \\ &= 2\left(g_{Tij}\lambda_i^p - b_{Tij}\lambda_i^q \right. \\ &\quad \left. + k_{t\max}^2\lambda_{t1}^k - k_{t\min}^2\lambda_{t2}^k\right) \end{aligned} \quad (43)$$

$$\begin{aligned} H_{Hee}(m,j) &= H_{Hff}(m,j) \\ &= -g_{Tij}\left(\lambda_i^p + \lambda_j^p\right) + b_{Tij}\left(\lambda_i^q + \lambda_j^q\right) \end{aligned} \quad (44)$$

$$H_{Hef}(m,j) = b_{Tij}\left(\lambda_i^p - \lambda_j^p\right) + g_{Tij}\left(\lambda_i^q - \lambda_j^q\right) \quad (45)$$

$$H_{Hfe}(m,j) = -b_{Tij}\left(\lambda_i^p - \lambda_j^p\right) - g_{Tij}\left(\lambda_i^q - \lambda_j^q\right) \quad (46)$$

$$H_{Hef}(m,i) = -\lambda_t^\theta \quad (47)$$

$$H_{Hfe}(m,i) = \lambda_t^\theta \quad (48)$$

where λ_j^p is the negative of $y(\cdot)$ associated with (19) ($\lambda_{N_s}^p = 1$); λ_j^q is the negative of $y(\cdot)$ associated with (20); λ_j^v is the $Z_1(\cdot)$ or the negative of the $Z_2(\cdot)$ associated with (25); λ_{t1}^k is the $Z_1(\cdot)$ associated with (22); λ_{t2}^k is the $Z_1(\cdot)$ associated with (23); and λ_t^θ is the negative of $y(\cdot)$ associated with (21).

For any Hessian $H_{Huv}(i,j)$ $(u, v \in \{e, f\})$ above

$$H_{Huv}(i,j) = \frac{\partial^2 L_\mu}{\partial u_i \partial v_j} = H_{Huv}(j,i).$$

B. ORPF Solution Procedure

An outline of the ORPF solution procedure is as follows:

Step 0) Initialize the optimization variables $\boldsymbol{X}$; the slack variables $\boldsymbol{S}_1$, $\boldsymbol{S}_2 \geq 0$; the Lagrange multipliers $\boldsymbol{y} \neq 0$, $\boldsymbol{Z}_1 \geq 0$, $\boldsymbol{Z}_2 \geq 0$; and the barrier parameter $\mu \geq 0$. Also set the max number of iteration $\boldsymbol{K}_{\max}$, initial iteration count $\boldsymbol{K} = 0$, and the convergence mismatch $\varepsilon_1 = \varepsilon_2 = 10^{-6}$.

Step 1) Calculate the constant Hessian matrices $\boldsymbol{H}_f(\boldsymbol{x})$, $\boldsymbol{H}_{g_j}(\boldsymbol{x})$, $\boldsymbol{H}_{h_{1j}}(\boldsymbol{x})$, and $\boldsymbol{H}_{h_{2j}}(\boldsymbol{x})$, as shown in part A.

Step 2) **Predicting process**. Neglect the barrier parameter and the second-order delta terms, and form and solve the predicting Newton system to obtain the affine scaling directions

$$\left[\Delta\boldsymbol{x}^{aff}, \Delta\boldsymbol{y}^{aff}, \Delta\boldsymbol{Z}_1^{aff}, \Delta\boldsymbol{Z}_2^{aff}, \Delta\boldsymbol{S}_1^{aff}, \Delta\boldsymbol{S}_2^{aff}\right].$$

Adjust μ and estimate the second-order delta terms by the affine scaling directions, and then form the correcting equation.

Step 3) **Correcting process**. Solve the correcting Newton system to obtain the actual search directions

$$[\Delta\boldsymbol{x}, \Delta\boldsymbol{y}, \Delta\boldsymbol{Z}_1, \Delta\boldsymbol{Z}_2, \Delta\boldsymbol{S}_1, \Delta\boldsymbol{S}_2].$$

Compute the step length in the search direction and update the primary and dual variables

$$[\boldsymbol{x}, \boldsymbol{y}, \boldsymbol{Z}_1, \boldsymbol{Z}_2, \boldsymbol{S}_1, \boldsymbol{S}_2].$$

Increment the iteration count, i.e., $\boldsymbol{K} = \boldsymbol{K} + 1$.

Step 4) If the following two convergence criteria are simultaneously satisfied, then output the result and stop. Otherwise, go to Step 2).

a) The complementary gap must be less than ε_1

$$\text{Gap} = \boldsymbol{h}_{1\max}^T\boldsymbol{Z}_1 + \boldsymbol{h}_{2\min}^T\boldsymbol{Z}_2 < \varepsilon_1.$$

b) The maximum norm of the KKT conditions must be less than ε_2

$$|\text{the largest mismatch of KKT}| < \varepsilon_2.$$

V. Simulation Result

The computational effort in each iteration of PCPDIPM is dominated by the solution of the linear system (32). It is vital to consider an efficient method for the solution. The coefficient matrix in (32) is asymmetric but highly sparse, so it is useful to adopt efficient sparse techniques for its ordering and factorization. MATLAB provides several sparse ordering functions for an asymmetric matrix. In this ORPF study, both the proposed and the conventional models are developed in MATLAB, including the sparse ordering function Column Approximate Minimum Degree (COLAMD) for the asymmetric matrix. IEEE Test Systems with 14, 30, 57, 118, and 300 buses and Chongqing practical systems with 171 and 1338 buses are implemented to verify the performance of the proposed method. The results are also compared with that from the conventional model. The only difference between the two models is that the LTC turns ratio variables are explicit in the conventional model, similar to [3], while the dummy nodal voltages replace those variables in the proposed model.

TABLE I
DIMENSIONS OF THE NLP PROBLEMS OF TEST SYSTEMS

System	N_B	N_L	N_T	N_G	N_{cr}	The Proposed Model			Conventional Model		
						r	p	n	r	p	n
IEEE14	14	20	3	2	1	20	30	63	20	27	60
IEEE30	30	41	4	6	9	49	63	141	49	59	137
IEEE57	57	80	6	7	3	73	119	248	73	113	242
IEEE118	118	186	9	36	14	177	244	538	177	235	529
Ch-171	171	223	42	10	45	268	383	821	268	341	779
IEEE300	300	411	43	57	12	412	642	1353	412	599	1310
S-1338	1338	1337	80	69	138	1597	2755	5689	1597	2675	5609

Legend:

N_B:the number of original system nodes
N_L:the number of system branches
N_T: the number of LTC branches
N_G:the number of the generator nodes
N_{cr}:the number of reactive compensation nodes
r: number of inequality constraints
p: number of equality constraints
n: size of the Newton linear system

TABLE II
TOTAL CPU TIME (S) FOR FORMING THE $\boldsymbol{H}_H$

System Name	The proposed Model	Conventional Model
IEEE14	0.0230	0.0460
IEEE30	0.0300	0.1250
IEEE57	0.0650	0.1320
IEEE118	0.1090	0.2810
Ch-171	0.2160	0.4160
IEEE300	0.5000	0.9980
S-1338	3.0300	5.3990

TABLE III
TOTAL CPU TIME (S) FOR SOLVING EQUATION (32)

System Name	The Proposed Model	Conventional Model
IEEE14	0.0250	0.0100
IEEE30	0.0770	0.0450
IEEE57	0.0820	0.0630
IEEE118	0.2970	0.2250
Ch-171	0.3610	0.2490
IEEE300	1.0080	0.9350
S-1338	2.6680	2.2630

Table I displays the corresponding dimensions of the nonlinear programming (NLP) problems of the seven test systems. It can be seen that the number of the equality constraints and the size of the Newton system are both higher than that of the conventional model by N_T (the number of the LTCs).

Table II displays the total CPU times for forming the Hessian $\boldsymbol{H}_H$ in the entire iterations for both the proposed and conventional model. It can be seen that the time needed for the proposed model is less than that for the conventional model. The Hessians composing $\boldsymbol{H}_H$ are constant in the proposed model and need to be formed just once in the entire iteration process. However, some elements in the Hessians corresponding to the LTC tap ratios need to be computed in each iteration for the conventional one.

Table III lists the total CPU times for solving the Newton system (32) in the entire iterations for both the proposed and conventional model. The results show that the time needed by the proposed model is slightly higher than that by the conventional model. This is because of the introduction of the dummy nodes into the system in the proposed model, which results in an increase in the size of the Newton system. However, from Tables II and III, it can be observed that the time saved by the proposed model in calculating the $\boldsymbol{H}_H$ is longer than that increased in solving the larger Newton system.

TABLE IV
TIMES, ITERATIONS, AND POWER LOSSES

System Name	Times for M1 (S)	Times for M2 (S)	Iterations	Power Losses (pu)
IEEE14	0.0780	0.0780	8	0.1291
IEEE30	0.1400	0.1720	10	0.0682
IEEE57	0.2500	0.2970	9	0.2605
IEEE118	0.6250	0.8580	12	1.1367
Ch-171	0.8280	1.1250	13	0.5197
IEEE300	1.9040	2.5310	14	3.5467
S-1338	7.8790	9.8750	16	0.5976

TABLE V
POWER LOSSES DURING THE ITERATIVE PROCESS

Iteration	P_L for IEEE 14		P_L for IEEE 57		P_L for IEEE 300	
	M1	M2	M1	M2	M1	M2
1	-2.1900	-2.1900	-3.9580	-3.9580	-0.4642	-0.4642
2	0.1480	0.1457	-0.1960	-0.1675	-0.0067	-0.0107
3	0.1332	0.1346	0.2597	0.2590	2.7733	2.8875
4	0.1334	0.1324	0.2619	0.2622	3.9737	3.9813
5	0.1283	0.1283	0.2604	0.2604	3.8016	3.7965
6	0.1290	0.1291	0.2605	0.2605	3.6203	3.6217
7	0.1291	0.1291	0.2605	0.2605	3.5590	3.5617
8	0.1291	0.1291	0.2605	0.2605	3.5498	3.5502
9			0.2605	0.2605	3.5476	3.5480
10					3.5469	3.5469
11					3.5467	3.5467
12					3.5467	3.5467
13					3.5467	3.5467
14					3.5467	3.5467

Legend:

M1: Proposed model
M2: Conventional model
P_L : Power Losses

Table IV lists the total CPU time for solving the ORPF with the proposed model (M1) and the conventional model (M2), the number of iterations for the convergence, and the power losses. The total time includes the entire time that is needed for forming the Hessians, the Jacobians, and the coefficient matrix and for solving the Newton system, etc. The table indicates an interesting result that both the proposed and the conventional models produce the same optimal losses and iteration counts in all seven test cases. However, the total calculation time needed for the proposed model is always shorter than that for the conventional model for the seven test cases; the larger the size of the system, the more the reduction in the total calculation time.

To further explore the convergence characteristics of the proposed method, the changes in power losses during the iterative process are observed and compared with that obtained in the conventional method. Table V lists the optimal power losses (P_L) during the iterative process for three test systems IEEE 14, IEEE 57, and IEEE 300. The results show that the two models exhibit similar convergence characteristics. The power losses obtained from the two models differ a little bit in the first several iterations, but they converge to the same final value with the same iteration count for a particular test system under consideration.

From the above result, it can be seen that the proposed model, by modifying the conventional model slightly, is able to obtain the same optimal results in the identical iteration counts but at a much faster speed.

VI. Conclusion

A new improved ORPF model in the rectangular coordinate is presented in this paper. In this model, the LTC transformer branch is represented by an ideal transformer and its series impedance with a dummy node located between them. The voltages of the two sides of the ideal transformer are used to replace the turn ratio of the LTC so that the ORPF model becomes quadratic. The Hessian matrices in this model are constants, and they need to be calculated only once in the entire optimization process. The extra dummy nodes introduced into the system increase the number of variables and constraints, which results in a slightly longer time for solving the larger Newton system. However, the time saved because of the emergence of the constant Hessians in the new ORPF model is much longer than the time that increased in solving the larger Newton system. Seven example systems, ranging from 14 buses to 1338 buses, are implemented to demonstrate the validity and effectiveness of the model. The results indicate that the proposed ORPF model, by modifying the conventional model slightly, is able to obtain the same optimal results in the identical iteration counts but at a much faster speed.

Appendix

The angles of the voltages at the high voltage node i and the dummy node m of the LTC branch in Fig. 3 are equal

$$arctg\left(\frac{f_i}{e_i}\right) = arctg\left(\frac{f_m}{e_m}\right).$$

So

$$e_i f_m - e_m f_i = 0.$$

Therefore, for all the branches from $j = 1, \ldots, N_T$

$$g_{\theta j}(\mathbf{x}) = e_i f_m - e_m f_i = 0 \quad j = 1, \cdots, N_T. \tag{21}$$

From the LTC tap ratio bounds, $k_{t\min} \le k_t \le k_{t\max}$. Replacing $k_t = \sqrt{(e_i^2 + f_i^2)/(e_m^2 + f_m^2)}$, taking the upper and lower bounds, and squaring both sides

$$\begin{aligned} 0 &\le k_{t\max}^2 \left(e_m^2 + f_m^2\right) - \left(e_i^2 + f_i^2\right) \\ 0 &\le \left(e_i^2 + f_i^2\right) - k_{t\min}^2 \left(e_m^2 + f_m^2\right). \end{aligned}$$

The generalized forms of these inequality functions are (22) and (23).

$$\begin{aligned} 0 \le h_{kj}(\mathbf{x}) &= k_{t\max}^2 \left(e_m^2 + f_m^2\right) - \left(e_i^2 + f_i^2\right) \quad j = 1, \cdots, N_T \\ 0 \le h_{kj}(\mathbf{x}) &= \left(e_i^2 + f_i^2\right) - k_{t\min}^2 \left(e_m^2 + f_m^2\right) \quad j = 1, \cdots, N_T. \end{aligned}$$

References

[1] H. Wei, H. Sasaki, and J. Kubokawa, "An interior point nonlinear programming for optimal power flow problems with a novel data structure [J]," *IEEE Trans. Power Syst.*, vol. 13, no. 3, pp. 870–877, Aug. 1997.

[2] M. Liu and S. K. Tao, "An extended nonlinear primal-dual interior-point algorithm for reactive-power optimization of large-scale power systems with discrete control variables [J]," *IEEE Trans. Power Syst.*, vol. 17, no. 4, pp. 982–991, Nov. 2002.

[3] G. L. Torres and V. H. Quintana, "An interior-point method for nonlinear optimal power flow using voltage rectangular coordinates [J]," *IEEE Trans. Power Syst.*, vol. 13, no. 4, pp. 1211–1218, Nov. 1998.

[4] ——, "On a nonlinear multiple-centrality-corrections interior-point method for optimal power flow [J]," *IEEE Trans. Power Syst.*, vol. 16, no. 2, pp. 222–228, May 2001.

[5] Y.-C. Wu, A. S. Debs, and R. E. Marsten, "A direct nonlinear predictor-corrector primal-dual interior point algorithm for optimal power flows [J]," *IEEE Trans. Power Syst.*, vol. 9, no. 2, pp. 876–883, May 1994.

[6] D. I. Sun, B. Ashley, B. Brewer, A. Hughes, and W. F. Tinney, "Optimal power flow by Newton approach [J]," *IEEE Trans. Power App. Syst*, vol. PAS-103, no. 10, pp. 2864–2880, Oct. 1984.

[7] H. Wei, H. Sasaki, and J. Yokoyama, "An application of interior point quadratic programming algorithm to power system optimization problems [J]," *IEEE Trans. Power Syst.*, vol. 11, no. 1, pp. 260–266, Feb. 1996.

[8] P. Heggernes, S. C. Eisenstat, G. Kumfert, A. Pothen, and A. Pothen, "The Computational Complexity of the Minimum Degree Algorithm [R],", ICASE Rep. no. 2001-42.

[9] W. F. Tinney and J. W. Walker, "Direct solutions of sparse network equations by optimally ordered triangular factorization," *Proc. IEEE*, vol. JROC-55, no. 11, pp. 1801–1809, Nov. 1967.

[10] W. Xiaodong, L. Naihu, and D. Qia, "A primal-dual interior point method for optimal voltage/reactive power control with sparsity structure) [J]," *Power Syst. Technol.*, vol. 23, no. 3, pp. 23–26, 1999.

[11] M. J. Rider, V. L. Paucar, and A. V. Garcia, "Enhanced higher-order interior-point method to minimize active power losses in electric energy systems [J]," *Proc. Inst. Elect. Eng., Gener., Transm., Distrib.*, vol. 151, no. 4, pp. 517–525, Jul. 2004.

[12] W. Rosehart and J. A. Aguado, "Alternative optimal power flow formulations," in *Proc. 14th Power System Computation Conf.*, Seville, Spain, 2002, Session 41, Paper 4.

Wei Yan received the Ph.D. degree in electrical engineering from Chongqing University, Chongqing, China, in 1999.

Currently, he is an Associate Professor and Associate Chairman of the Electrical Power Department, Electrical Engineering College, Chongqing University. His research interests include optimal operation and control in power systems.

Juan Yu was born in Jingzhou, China, on December 17, 1980. She received the B.S. degree in electrical engineering from Chongqing University, Chongqing, China, in 2002. Currently, she is a working toward the Ph.D. degree in electrical engineering from Chongqing University.

Her research interests include reactive optimal problem and state estimation in power systems.

David C. Yu received the Ph.D. degree in electrical engineering from the University of Oklahoma, Norman, in 1983.

Currently, he is a Professor in the Department of Electrical Engineering and Computer Science, University of Wisconsin, Milwaukee. His research interests include power systems software development and distribution system analysis.

Kalu Bhattarai received the B.E. degree in electrical engineering from Tianjin University, Tianjin, China, in 1994. Currently, he is working toward the M.E. degree in the Department of Electrical Engineering and Computer Science, University of Wisconsin, Milwaukee.